Pergamon

Int. J. Solids Structures Vol. 33, No. 4, pp. 595–608, 1996

0020-7683/96 $9.50 + .00

0020-7683(94)00243-6

TRACING EQUILIBRIUM PATHS OF ELASTIC PLATES UNDER DIFFERENT LOADING PATHS

CHANG-GEN DENG
College of Structural Engineering, Tongji University, Shanghai 200092, People's Republic of China

(*Received* 14 *April* 1993; *in revised form* 20 *September* 1994)

Abstract—A new algorithm for tracing equilibrium paths of simply supported rectangular thin plates in the nonlinear elastic range under different loading paths is developed. In the algorithm, different loading paths are expressed as different functions of path parameter $t \in [0, 1]$; the nonlinear algebraic equilibrium equations are derived by a semi-analytical method and solved by applying Broyden's method; locating critical points is realized by applying a determinant-based bisection method; tracing primary equilibrium paths and bifurcated equilibrium paths is controlled by specifying the incremental arc length of the paths; and switching from primary equilibrium paths to bifurcated equilibrium paths at bifurcation points is controlled by specifying the incremental amplitude of critical modes. The algorithm is applied in some representative examples of imperfect plates under six different loading paths of inplane compressive stresses and transverse load. Through these examples, the following phenomena are observed: different loading paths sometimes lead to different final equilibrium states; under some loading paths with special final loads, there exist bifurcation points on fundamental equilibrium paths even for imperfect plates, and through a bifurcation point there are two stable bifurcated equilibrium paths which approach different final equilibrium states.

1. INTRODUCTION

Practical engineering structures and members are usually subject to multiple-parameter conservative loading, i.e. the loading consists of a number of independently varying conservative loads, e.g. beam-columns under axial compressive forces and transverse loads, thin plates under inplane loads and transverse loads, shallow spherical shells under boundary inplane compressive forces and normal compressive forces, etc. There are many different loading paths on which these loads are applied to some specified final magnitudes. For example, the proportional loading path on which all loads increase simultaneously and gradually from zero to their final magnitudes is one single-parameter loading path; the alternative loading path on which all loads increase separately and successively from zero to their final magnitudes is another single-parameter loading path. If all loading parameters vary independently, and if overloading and unloading are allowed, it is evident that there are an infinite number of different loading paths.

In the elasto–plastic range, it is well known that different loading paths always lead to different final equilibrium states and different limit load-bearing capacities of a structure. In the nonlinear elastic range, it has also been observed in experimental and theoretical studies that different loading paths sometimes lead to different final equilibrium states for certain structure–final load combinations. Studies have revealed that the root cause for different loading paths leading to different final equilibrium states is the solution multiplicity in nonlinear problems.

It is quite common that certain structures which are susceptible to buckling can possess multiple equilibrium states under the same loading levels [Thompson (1984); Maaskant and Roorda (1992)]. For nonlinear stability analysis of these structures, tracing equilibrium paths facilitates the location of the real final equilibrium states; tracing equilibrium paths in the elastic range provides correct initial conditions for elasto–plastic analysis and then ensures correctly tracing equilibrium paths in the elasto–plastic range and correctly evaluating limit load–bearing capacities. Therefore, tracing equilibrium paths in the elastic range is fundamental and necessary.

Tracing equilibrium paths also contributes to understanding mode jumping. Mode jumping of plates is a well-known phenomenon observed in extensive experimental and theoretical studies. Maaskant and Roorda (1992) have studied mode jumping by considering the two-mode interaction of simply supported rectangular plates under biaxial loading. Their analysis has illustrated that different loading conditions sensitively influence the mode-jumping phenomenon and qualitatively change the postbuckling behaviour. Also considering only two-mode interaction, Wicks (1988) has studied the mode jumping of a simply supported rectangular plate under uniaxial inplane compression, with a trapezoidally distributed transverse pressure being used to generate the imperfection. His study has shown that the postbuckling behaviour is sensitive to the type of transverse pressure (whether it is symmetric or not), i.e. the postbuckling behaviour is sensitive to the mode of initial imperfection.

In this paper, for tracing equilibrium paths of simply supported rectangular thin plates in the nonlinear elastic range under different loading paths, a new algorithm is developed. Besides manipulating different loading paths, the algorithm is valid in all the following phases of tracing equilibrium paths: tracing primary equilibrium paths, locating critical (limit or bifurcation) points, switching from primary equilibrium paths to bifurcated equilibrium paths, tracing bifurcated equilibrium paths, and switching from one segment of loading paths to another. In the algorithm, different loading paths are expressed as different functions of path parameter; the number of interacting modes may be selected to be greater than two; and different modes of initial deflection and of transverse load may be included.

To demonstrate its versatility and validity, the algorithm is also applied in some representative examples of imperfect plates under three typical piecewise linear loading paths of uniaxial compressive stress and transverse load, and three of biaxial compressive stresses. Through these examples, some instructive phenomena are observed.

2. THE NONLINEAR ALGEBRAIC EQUILIBRIUM EQUATIONS

To trace equilibrium paths of simply supported rectangular thin plates in the elastic range, the nonlinear algebraic equilibrium equations with respect to deflection amplitudes must be derived first. The governing differential equations of an elastic plate subject to boundary inplane compressive stresses p_x, p_y and transverse load q in the postbuckling range are (Chia, 1980)

$$\begin{cases} D\nabla^2\nabla^2 w = q + hL(\varphi, w + w_0), \\ \dfrac{1}{E}\nabla^2\nabla^2\varphi = \dfrac{1}{2}[L(w + w_0, w + w_0) - L(w_0, w_0)], \end{cases} \tag{1}$$

where $D = Eh^3/[12(1-\mu^2)]$ is the bending stiffness of the plate, in which E is Young's modulus and μ is Poisson's ratio; a, b and h are the length, width and thickness of the plate, respectively; w_0, w, $W = w + w_0$ denote the initial deflection, induced deflection and total deflection of the plate, respectively; φ denotes the stress function of the plate, with the inplane tensile stresses and shearing stress being evaluated as $\sigma_x = \partial^2\varphi/\partial y^2$, $\sigma_y = \partial^2\varphi/\partial x^2$, $\tau_{xy} = -\partial^2\varphi/\partial x\,\partial y$, respectively; $\nabla^2\nabla^2$ is the biharmonic differential operator; and $L(\varphi, w)$ is the differential operator defined as

$$L(\varphi, w) = \frac{\partial^2\varphi}{\partial x^2}\frac{\partial^2 w}{\partial y^2} + \frac{\partial^2\varphi}{\partial y^2}\frac{\partial^2 w}{\partial x^2} - 2\frac{\partial^2\varphi}{\partial x\,\partial y}\frac{\partial^2 w}{\partial x\,\partial y}. \tag{2}$$

The total deflection and initial deflection are assumed as

$$W = w + w_0 = \sum_{i=1}^{N_1} W_i \sin \alpha_i x \sin \beta_i y, \quad w_0 = \sum_{i=1}^{N_1} w_{0i} \sin \alpha_i x \sin \beta_i y, \tag{3}$$

which satisfy the boundary conditions for deflections, i.e. simply supported at all sides of the rectangular plate. The distributed transverse load may be expanded as the following double Fourier series cut off up to N_2 items (Chia, 1980)

$$q = \sum_{i=1}^{N_2} q_i \sin \alpha_i x \sin \beta_i y. \tag{4}$$

In expressions (3) and (4),

$$\alpha_i = \frac{m_i \pi}{a}, \quad \beta_i = \frac{n_i \pi}{b}, \quad (\alpha_i, \beta_i) \neq (\alpha_j, \beta_j) \quad \text{if } i \neq j, \quad (i, j = 1, 2, \ldots, N), \quad N = \max(N_1, N_2), \tag{5}$$

where m_i, m_j, n_i, n_j, etc., are positive integers.

Remark 1. For a fixed number M_1 of modes of the initial deflection, a comparable number N_1 (e.g. $N_1 \geqslant 3M_1$) of modes of the induced deflection can give very accurate results. It is understood that in eqn (3) $w_{0i} = 0$, $(i = M_1 + 1, \ldots, N_1)$ for conciseness. By the same argument, the number N_2 of items in the approximate expression (4) of the transverse load is set to be $N_2 = N_1 = N$, which is assumed in what follows.

The deflections (3) being substituted into the second of eqns (1), i.e. the differential compatibility equation, the stress function φ is solved as

$$\varphi = -\frac{p_x}{2} y^2 - \frac{p_y}{2} x^2 - \frac{E}{8} \sum_{i=1}^{N} \sum_{j=1}^{N} (W_i W_j - w_{0i} w_{0j}) \times \sum_{\xi=-1,1} \sum_{\eta=-1,1} \frac{\xi\eta(\alpha_i \beta_j - \xi\eta \alpha_j \beta_i)^2}{[(\alpha_i + \xi\alpha_j)^2 + (\beta_i + \eta\beta_j)^2]^2} \cos(\alpha_i + \xi\alpha_j) x \cos(\beta_i + \eta\beta_j) y. \tag{6}$$

It is verified that the stress function φ satisfies the following inplane conditions:

(a) parallel straight opposite sides, i.e.

$$u|_{x=a} - u|_{x=0} = \int_0^a \left[\frac{1}{E} \left(\frac{\partial^2 \varphi}{\partial y^2} - \mu \frac{\partial^2 \varphi}{\partial x^2} \right) - \frac{1}{2} \left(\frac{\partial W}{\partial x} \right)^2 + \frac{1}{2} \left(\frac{\partial w_0}{\partial x} \right)^2 \right] dx = -\frac{a(p_x - \mu p_y)}{E},$$

$$v|_{y=b} - v|_{y=0} = \int_0^b \left[\frac{1}{E} \left(\frac{\partial^2 \varphi}{\partial x^2} - \mu \frac{\partial^2 \varphi}{\partial y^2} \right) - \frac{1}{2} \left(\frac{\partial W}{\partial y} \right)^2 + \frac{1}{2} \left(\frac{\partial w_0}{\partial y} \right)^2 \right] dy = -\frac{b(p_y - \mu p_x)}{E}.$$

(b) specified average normal stresses and zero shearing stresses at the boundaries, i.e.

$$\int_0^b \sigma_x|_{x=0} \, dy \cdot b = \int_0^b \sigma_x|_{x=a} \, dy \cdot b = -p_x,$$

$$\int_0^a \sigma_y|_{y=0} \, dx \cdot a = \int_0^a \sigma_y|_{y=b} \, dx \cdot a = -p_y,$$

$$\tau_{xy}|_{x=0} = \tau_{xy}|_{x=a} = \tau_{xy}|_{y=0} = \tau_{xy}|_{y=b} = 0.$$

The deflections (3), the transverse load (4) and the stress function (6) being substituted

into the first of eqns (1), i.e. the differential equilibrium equation, the algebraic equilibrium equations are derived by Galerkin's method as

$$D\left(\frac{\pi}{b}\right)^4\left[\left(\frac{m_i}{\gamma}\right)^2+n_i^2\right]^2(W_i-w_{0i})-q_i-h\left(\frac{\pi}{b}\right)^2\left[p_x\left(\frac{m_i}{\gamma}\right)^2+p_y n_i^2\right]W_i$$

$$+\sum_{j=1}^{N}\sum_{k=1}^{N}\sum_{l=1}^{N}\frac{Eh}{32\gamma^4}\left(\frac{\pi}{b}\right)^4 W_j(W_k W_l-w_{0k}w_{0l})R_{ijkl}=0,\quad (i=1,2,\ldots,N), \tag{7}$$

where $\gamma=a/b$ is the aspect ratio of the plate, and

$$R_{ijkl}=\sum_{\xi=-1,1}\sum_{\eta=-1,1}(S_{ijkl}^{\xi\eta}+T_{ijkl}^{\xi\eta})\,[(m_i+\xi m_k)^2/\gamma^2+(n_j+\eta n_k)^2]^2, \tag{8}$$

$$S_{ijkl}^{\xi\eta}=\xi\eta[(m_k+\xi m_l)^2n_j^2+(n_k+\eta n_l)^2m_j^2](m_k n_l-\xi\eta m_l n_k)^2$$
$$\times H(m_k+\xi m_l,m_j,m_i)H(n_k+\eta n_l,n_j,n_i), \tag{9}$$

$$T_{ijkl}^{\xi\eta}=-2\xi\eta[(m_k+\xi m_l)n_j(n_k+\eta n_l)m_j](m_k n_l-\xi\eta m_l n_k)^2$$
$$\times H(m_j,m_k+\xi m_l,m_i)H(n_j,n_k+\eta n_l,n_i), \tag{10}$$

$$H(\omega_1,\omega_2,\omega_3)=4\int_0^1\cos\omega_1\pi\zeta\sin\omega_2\pi\zeta\sin\omega_3\pi\zeta\,\mathrm{d}\zeta$$
$$=\begin{cases}2, & \omega_2-\omega_3=\omega_1=0;\\ -2, & \omega_2+\omega_3=\omega_1=0;\\ 1, & \pm(\omega_2-\omega_3)=\omega_1\neq 0;\\ -1, & \pm(\omega_2+\omega_3)=\omega_1\neq 0;\\ 0, & \text{otherwise.}\end{cases} \tag{11}$$

From the definition of the following nondimensional quantities:

$$\bar{D}=\frac{D}{Eh^3},\quad \bar{W}_i=\frac{W_i}{h},\quad \bar{w}_{0i}=\frac{w_{0i}}{h},\quad \bar{p}_x=\frac{p_x hb^2}{\pi^2 D},\quad \bar{p}_y=\frac{p_y hb^2}{\pi^2 D},\quad \bar{q}_i=\frac{q_i b^4}{\pi^4 Dh}, \tag{12}$$

the algebraic equilibrium equations are nondimensionalized as

$$\left[\left(\frac{m_i}{\gamma}\right)^2+n_i^2\right]^2(\bar{W}_i-\bar{w}_{0i})-\bar{q}_i-\left[\bar{p}_x\left(\frac{m_i}{\gamma}\right)^2+\bar{p}_y n_i^2\right]\bar{W}_i$$

$$+\sum_{j=1}^{N}\sum_{k=1}^{N}\sum_{l=1}^{N}\frac{1}{32\bar{D}\gamma^4}\bar{W}_j(\bar{W}_k\bar{W}_l-\bar{w}_{0k}\bar{w}_{0l})R_{ijkl}=0,\quad (i=1,2,\ldots,N). \tag{13}$$

Remark 2. Although the nonlinear algebraic equilibrium equations are derived by the above semi-analytical method approximately, the accuracy may attain any required level by selecting an appropriate number N. In examples hereinafter, the number is selected increasingly and the convergence is tested to ensure the accuracy. Because any number of interacting modes may be included in this analysis, the accuracy is expected to be higher

than that in Maaskant and Roorda (1992) and Wicks (1988), where only two interacting modes are included.

3. DIFFERENT LOADING PATHS

To describe different loading paths, a nondimensional time parameter $t \in [0, 1]$ which is taken for the path parameter is introduced, with the application of loading beginning at time $t = 0$ and ending at time $t = 1$ when reaching final loads. Time $t = 1$ may correspond to any finite "long time", e.g. 10 minutes, 10 hours, etc. Therefore, it is reasonable to consider the loads being applied very slowly and to treat them as quasi-static loads.

Different loading paths are described by expressing loading parameters as different functions of the time parameter. These loading paths all approach the final loading parameters, which represent final loads at time $t = 1$. Herein $\bar{p}_x$ and $\bar{p}_y$ denote nondimensional inplane loading parameters, and $\bar{p}_z$ denotes the nondimensional transverse loading parameter, which is defined by

$$\bar{q}_i = \bar{p}_z \bar{q}_{0i} \quad (i = 1, 2, \ldots, N). \tag{14}$$

where $\bar{q}_{0i}$ are normalized ($\max \bar{q}_{0i} = 1$) relative magnitudes of the transverse loads; $\bar{p}_x^*$, $\bar{p}_y^*$ and $\bar{p}_z^*$ denote the corresponding final loading parameters. Similarly, $\bar{W}_i$ represent equilibrium states and $\bar{W}_i^*$ represent final equilibrium states.

In this paper, only piecewise linear loading paths of the following form are considered:

$$\bar{p}_x = \bar{p}_x^{(0)} + \bar{p}_x^{(1)} t, \quad \bar{p}_y = \bar{p}_y^{(0)} + \bar{p}_y^{(1)} t, \quad \bar{p}_z = \bar{p}_z^{(0)} + \bar{p}_z^{(1)} t, \quad t \in [0, 1]. \tag{15}$$

To investigate the influence of different loading paths of uniaxial compressive stress and transverse load on the final equilibrium states, $\bar{p}_y = 0$ is assumed. Three typical piecewise linear loading paths of $\bar{p}_x$, $\bar{p}_z$ are considered. On the proportional loading path I, $\bar{p}_x$ and $\bar{p}_z$ are applied simultaneously from zero to $\bar{p}_x^*, \bar{p}_z^*$. On the alternative loading path II, $\bar{p}_x$ is applied firstly from zero to $\bar{p}_x^*$ (the first segment), and $\bar{p}_z$ is applied secondly from zero to $\bar{p}_z^*$ (the second segment). On another alternative loading path III, $\bar{p}_z$ is applied firstly from zero to $\bar{p}_z^*$ (the first segment), and $\bar{p}_x$ is applied secondly from zero to $\bar{p}_x^*$ (the second segment).

(1) Loading path I

$$\begin{cases} \bar{p}_x^{(0)} = 0, & \bar{p}_y^{(0)} = 0, & \bar{p}_z^{(0)} = 0, \\ \bar{p}_x^{(1)} = \bar{p}_x^*, & \bar{p}_y^{(1)} = 0, & \bar{p}_z^{(1)} = \bar{p}_z^*, \end{cases} \quad t \in [0, 1]. \tag{16}$$

(2) Loading path II

$$\begin{cases} \bar{p}_x^{(0)} = 0, & \bar{p}_y^{(0)} = 0, & \bar{p}_z^{(0)} = 0, \\ \bar{p}_x^{(1)} = 2\bar{p}_x^*, & \bar{p}_y^{(1)} = 0, & \bar{p}_z^{(1)} = 0, \end{cases} \quad t \in [0, 1/2]; \tag{17}$$

$$\begin{cases} \bar{p}_x^{(0)} = \bar{p}_x^*, & \bar{p}_y^{(0)} = 0, & \bar{p}_z^{(0)} = -\bar{p}_z^*, \\ \bar{p}_x^{(1)} = 0, & \bar{p}_y^{(1)} = 0, & \bar{p}_z^{(1)} = 2\bar{p}_z^*, \end{cases} \quad t \in [1/2, 1]. \tag{18}$$

(3) Loading path III

$$\begin{cases} \bar{p}_x^{(0)} = 0, & \bar{p}_y^{(0)} = 0, & \bar{p}_z^{(0)} = 0, \\ \bar{p}_x^{(1)} = 0, & \bar{p}_y^{(1)} = 0, & \bar{p}_z^{(1)} = 2\bar{p}_z^*, \end{cases} \quad t \in [0, 1/2]; \tag{19}$$

$$\begin{cases} \bar{p}_x^{(0)} = -\bar{p}_x^*, & \bar{p}_y^{(0)} = 0, & \bar{p}_z^{(0)} = \bar{p}_z^*, \\ \bar{p}_x^{(1)} = 2\bar{p}_x^*, & \bar{p}_y^{(1)} = 0, & \bar{p}_z^{(1)} = 0, \end{cases} \quad t \in [1/2, 1]. \tag{20}$$

To investigate the influence of different loading paths of biaxial compressive stresses on the final equilibrium states, $\bar{p}_z = 0$ and then $\bar{q}_i = 0$ $(i = 1, 2, \ldots, N)$ are assumed. Three typical piecewise linear loading paths of $\bar{p}_x$, $\bar{p}_y$ are also considered. On the proportional loading path IV, $\bar{p}_x$ and $\bar{p}_y$ are applied simultaneously from zero to $\bar{p}_x^*, \bar{p}_y^*$. On the alternative loading path V, $\bar{p}_x$ is applied firstly from zero to $\bar{p}_x^*$ (the first segment), and $\bar{p}_y$ is applied secondly from zero to $\bar{p}_y^*$ (the second segment). On another alternative loading path VI, $\bar{p}_y$ is applied firstly from zero to $\bar{p}_y^*$ (the first segment), and $\bar{p}_x$ is applied secondly from zero to $\bar{p}_x^*$ (the second segment).

(4) Loading path IV

$$\begin{cases} \bar{p}_x^{(0)} = 0, & \bar{p}_y^{(0)} = 0, & \bar{p}_z^{(0)} = 0, \\ \bar{p}_x^{(1)} = \bar{p}_x^*, & \bar{p}_y^{(1)} = \bar{p}_y^*, & \bar{p}_z^{(1)} = 0, \end{cases} \quad t \in [0, 1]. \tag{21}$$

(5) Loading path V

$$\begin{cases} \bar{p}_x^{(0)} = 0, & \bar{p}_y^{(0)} = 0, & \bar{p}_z^{(0)} = 0, \\ \bar{p}_x^{(1)} = 2\bar{p}_x^*, & \bar{p}_y^{(1)} = 0, & \bar{p}_z^{(1)} = 0, \end{cases} \quad t \in [0, 1/2]; \tag{22}$$

$$\begin{cases} \bar{p}_x^{(0)} = \bar{p}_x^*, & \bar{p}_y^{(0)} = -\bar{p}_y^*, & \bar{p}_z^{(0)} = 0, \\ \bar{p}_x^{(1)} = 0, & \bar{p}_y^{(1)} = 2\bar{p}_y^*, & \bar{p}_z^{(1)} = 0, \end{cases} \quad t \in [1/2, 1]. \tag{23}$$

(6) Loading path VI

$$\begin{cases} \bar{p}_x^{(0)} = 0, & \bar{p}_y^{(0)} = 0, & \bar{p}_z^{(0)} = 0, \\ \bar{p}_x^{(1)} = 0, & \bar{p}_y^{(1)} = 2\bar{p}_y^*, & \bar{p}_z^{(1)} = 0, \end{cases} \quad t \in [0, 1/2]; \tag{24}$$

$$\begin{cases} \bar{p}_x^{(0)} = -\bar{p}_x^*, & \bar{p}_y^{(0)} = \bar{p}_y^*, & \bar{p}_z^{(0)} = 0, \\ \bar{p}_x^{(1)} = 2\bar{p}_x^*, & \bar{p}_y^{(1)} = 0, & \bar{p}_z^{(1)} = 0, \end{cases} \quad t \in [1/2, 1]. \tag{25}$$

4. THE ALGORITHM FOR TRACING EQUILIBRIUM PATHS

An integrated algorithm for tracing equilibrium paths will be described below. Three sub-algorithms are integrated in the integrated algorithm, i.e. the sub-algorithm for solving the nonlinear algebraic equilibrium equations by applying Broyden's method, the sub-algorithm for locating bifurcation points by applying a determinant-based bisection method, the sub-algorithm for tracing primary equilibrium paths and bifurcated equilibrium paths by specifying the incremental arc length of the paths, and for switching from primary equilibrium paths to bifurcated equilibrium paths at bifurcation points by specifying the incremental amplitude of critical modes.

4.1. *Preparations*

After expressions (14)–(25) for the loading parameters $\bar{p}_x$, $\bar{p}_y$, $\bar{p}_z$ on different loading paths have been substituted into eqns (13), eqns (13) can be rearranged as follows:

$$F_i = B_i + B_{ij}u_M + B_{ij0}u_j + B_{ijk}u_j u_M + \sum_{k=1}^{N} B_{ijk}u_j u_k + \sum_{k=1}^{N}\sum_{j=1}^{N} B_{ijk}u_j u_k u_l = 0,$$

$$(i = 1, 2, \ldots, N), \quad (26)$$

where

$$u_i = \bar{W}_i, \quad u_M = t, \quad (i = 1, 2, \ldots, N)(M = N+1); \quad (27)$$

$$B_i = -\bar{p}_z^{(0)}\bar{q}_{0i} - [(m_i\gamma)^2 + n_i^2]^2\bar{w}_{0i}, \quad B_{ij} = -\bar{p}_z^{(1)}\bar{q}_{0i}, \quad (i = 1, 2, \ldots, N); \quad (28)$$

$$B_{ij0} = -(m_i\gamma)^2\bar{p}_x^{(0)} - n_i^2\bar{p}_y^{(0)}, \quad B_{ijj} = -(m_i\gamma)^2\bar{p}_x^{(1)} - n_i^2\bar{p}_y^{(1)}, \quad (i = 1, 2, \ldots, N); \quad (29)$$

$$B_{ij} = [(m_i\gamma)^2 + n_i^2]^2\delta_{ij} - \sum_{k=1}^{N}\sum_{l=1}^{N} B_{ijkl}\bar{w}_{0k}\bar{w}_{0l}, \quad (i, j = 1, 2, \ldots, N); \quad (30)$$

$$B_{ijkl} = R_{ijkl}(32\bar{D}_r^4), \quad (i, j, k, l = 1, 2, \ldots, N); \quad (31)$$

and δ_{ij} is the Kronecker delta: $\delta_{ij} = 0$ if $i \neq j$; $\delta_{ij} = 1$ if $i = j$.

Through solving eqns (26) for different time parameters $t \in [0, 1]$, equilibrium states $\bar{W}_i$ at any time t are determined. The loci of these equilibrium states make up equilibrium paths corresponding to the loading paths. The equilibrium paths which connect the initial state $\bar{w}_{0i}$ with the final equilibrium states $\bar{W}_i^*$ are the fundamental equilibrium paths which exist in reality. Hereinafter, tracing equilibrium paths means tracing the fundamental equilibrium paths.

The integrated algorithm requires an additional constraint equation $F_M = 0$ for tracing equilibrium paths, or for switching equilibrium paths at bifurcation points, or for locating bifurcation points or for solving equilibrium states under specified time parameters.

When tracing primary equilibrium paths or bifurcated equilibrium paths, the incremental arc length of the paths from time $t - \Delta t$ to time t is controlled to be Δs:

$$F_M = \sum_{i=1}^{M}(u_i - u_i^{t-\Delta t})^2 - (\Delta s)^2 = 0, \quad (32)$$

where superscripts $t - \Delta t$ and t represent evaluation at time $t - \Delta t$ and time t, respectively, and $\Delta t = u_M^t - u_M^{t-\Delta t}$ represents time increment.

When switching from primary equilibrium paths to bifurcated equilibrium paths at bifurcation points at time t, the incremental amplitude of the kth critical mode is controlled to be Δu_k:

$$F_M = (u_k - u_k^{t-\Delta t}) - \Delta u_k = 0, \quad (k \leqslant N), \quad (33)$$

where $\Delta u_k > 0$ corresponds to switching to one side of the bifurcated equilibrium paths and $\Delta u_k < 0$ corresponds to switching to the other side of the bifurcated equilibrium paths.

When locating bifurcation points or solving equilibrium states under a specified time parameter t_s, the constraint equation is as follows:

$$F_M = u_k^t - t_s = 0, \quad (k = M). \quad (34)$$

The integrated algorithm also requires formulation of the tangential stiffness matrix $\mathbf{K}^t$ and expanded tangential stiffness matrix $\bar{\mathbf{K}}^t$ at time t, which are defined as follows:

$$\mathbf{K}^t = [K_{ij}^t]_{N\times N}, \quad \bar{\mathbf{K}}^t = \begin{bmatrix} K_{ij}^t & K_{iM}^t \\ K_{Mj}^t & K_{MM}^t \end{bmatrix}_{M\times M}, \tag{35}$$

where

$$K_{ij}^t = \partial F_i/\partial u_j|^t = (B_{ij0} + B_{iji}u_M^t)\delta_{ij} + B_{ij} + \sum_{k=1}^{N}\sum_{l=1}^{N}(B_{ijkl} + B_{ikjl} + B_{ilkj})u_k^t u_l^t,$$

$$(i,j = 1,2,\ldots,N); \tag{36}$$

$$K_{iM}^t = \partial F_i/\partial u_M|^t = B_{ii} + B_{iii}u_i^t, \quad (i = 1,2,\ldots,N)(M = N+1); \tag{37}$$

$$K_{Mj}^t = \partial F_M/\partial u_j|^t = \begin{cases} 2(u_i^t - u_i^{t-\Delta t}), & \text{for } F_M = 0 \text{ as in eqn (32)}; \\ \delta_{jk}, & \text{for } F_M = 0 \text{ as in eqns (33) or (34)}; \end{cases}$$

$$(M = N+1)(j = 1,2,\ldots,N,M). \tag{38}$$

For conciseness, solution vector $\mathbf{u}$ and equation residual vector $\mathbf{F}$ are defined as follows:

$$\mathbf{u} = (u_1, u_2, \ldots, u_M)^{\mathrm{T}}, \quad \mathbf{F} = \mathbf{F}(\mathbf{u}) = (F_1, F_2, \ldots, F_M)^{\mathrm{T}}. \tag{39}$$

4.2. *Solving the nonlinear equilibrium equations*

The sub-algorithm for solving the nonlinear equilibrium equations $\mathbf{F}(\mathbf{u}) = \mathbf{0}$ after a load increment step, i.e. the step from time $t-\Delta t$ to time t, by Broyden's method [see, e.g., Dennis and Schnabel (1983)] is described below, where superscript l denotes the lth iteration loop number.

1°. For initial iteration loop $l = 0$, specify initial solution vector:

$$\mathbf{u}^{(0)} = \begin{cases} \mathbf{u}^{t-\Delta t} + e_M \Delta s, & \text{for } F_M = 0 \text{ as in eqn (32)}; \\ \mathbf{u}^{t-\Delta t} + e_k \Delta u_k, & \text{for } F_M = 0 \text{ as in eqns (33) or (34)}; \end{cases} \tag{40}$$

where $\mathbf{e}_i$, $(i = k, M)$ is the unit vector with the ith element being unit, and evaluate initial quasi-stiffness-matrix inverse:

$$\mathbf{A}^{(0)} = [\bar{\mathbf{K}}^{t-\Delta t}]^{-1}. \tag{41}$$

2°. Evaluate new solution vector:

$$\mathbf{u}^{(l+1)} = \mathbf{u}^{(l)} - \mathbf{A}^{(l)}\mathbf{F}^{(l)}. \tag{42}$$

3°. Evaluate new equation residual vector $\mathbf{F}^{(l+1)} = \mathbf{F}(\mathbf{u}^{(l+1)})$. If $\max_{i=1}^{M}|F_i^{(l+1)}| < \varepsilon$, then set $\mathbf{u}^t = \mathbf{u}^{(l+1)}$ and terminate the iteration.

4°. Evaluate incremental solution vector and incremental equation residual vector, respectively:

$$\Delta\mathbf{u}^{(l)} = \mathbf{u}^{(l+1)} - \mathbf{u}^{(l)}, \tag{43}$$

$$\Delta\mathbf{F}^{(l)} = \mathbf{F}^{(l+1)} - \mathbf{F}^{(l)}. \tag{44}$$

5°. Evaluate new quasi-stiffness-matrix inverse:

$$\mathbf{A}^{(l+1)} = \mathbf{A}^{(l)} + (\Delta\mathbf{u}^{(l)} - \mathbf{A}^{(l)}\Delta\mathbf{F}^{(l)})(\Delta\mathbf{u}^{(l)})^{\mathrm{T}}\mathbf{A}^{(l)}/C^{(l)}, \tag{45}$$

where

$$C^{(l)} = (\Delta\mathbf{u}^{(l)})^{\mathrm{T}}\mathbf{A}^{(l)}\Delta\mathbf{F}^{(l)} \neq 0, \tag{46}$$

then $l+1 \Rightarrow l$ and go to step 2 .

4.3. *Locating critical points*

Suppose there is a critical (limit or bifurcation) point **C** within a load step from time $t_l = t_r - \Delta t$ to time t_r, i.e., there is a solution $t = t_{cr}$ of the nonlinear determinant equation

$$D(t) = \det \mathbf{K}(t) = 0, \quad D(t_l)D(t_r) < 0, \quad t \in (t_l, t_r). \tag{47}$$

Any appropriate method which is capable of solving a unitary nonlinear equation may be applied. In this paper, the simple bisection method is used. The sub-algorithm for locating critical points is described below.

1 . Let $t = t_s = (t_l + t_r)/2$, choose $F_M = 0$ as in eqn (34) and solve the nonlinear equilibrium equations $\mathbf{F}(\mathbf{u}) = \mathbf{0}$ after the load step from time t_l to time t by Broyden's method.

2 . Calculate determinant $D(t) = \det \mathbf{K}^t$. If $|D(t)| \leqslant \varepsilon_1$ or $|t_r - t| \leqslant \varepsilon_2$, then terminate the iteration with critical point **C** being located as $\mathbf{u}_{cr} = \mathbf{u}^t$, $t_{cr} = t$.

3 . If $D(t)D(t_l) < 0$, then $t \Rightarrow t_r$, $D(t) \Rightarrow D(t_r)$; or else $t \Rightarrow t_l$, $D(t) \Rightarrow D(t_l)$. Go to step 1 .

4.4. *Tracing equilibrium paths and switching equilibrium paths*

The sub-algorithm for tracing equilibrium paths and switching equilibrium paths is described below.

1 . *Initialization.* For initial load step $t = 0$, specify initial solution vector as $\mathbf{u}^0 = (\bar{w}_{01}, \bar{w}_{02}, \ldots, \bar{w}_{0N}, 0)^{\mathrm{T}}$. Evaluate the initial stiffness matrix $\mathbf{K}^0$ and initial expanded stiffness matrix $\bar{\mathbf{K}}^0$, and calculate determinant $\det \mathbf{K}^0$.

2 . *Tracing primary equilibrium paths or bifurcated equilibrium paths.* $t + \Delta t \Rightarrow t$. Choose $F_M = 0$ as in eqn (32) and solve the nonlinear equilibrium equations $\mathbf{F}(\mathbf{u}) = \mathbf{0}$ after the load step from time $t - \Delta t$ to time t by Broyden's method.

3 . *Detecting critical points.* Calculate determinant $\det \mathbf{K}^t$. If $(\det \mathbf{K}^{t-\Delta t})(\det \mathbf{K}^t) > 0$, there is no critical point, then go to step 5 ; otherwise, there is a critical point within the load step from time $t_l = t - \Delta t$ to time $t_r = t$. If $(u_M^t - u_M^{t-\Delta t})(u_M^{t-\Delta t} - u_M^{(t-\Delta t)-\Delta t}) \leqslant 0$, the critical point is a limit point, or else the critical point is a bifurcation point.

4 . *Locating critical points and switching to bifurcated equilibrium paths.* Apply previously described bisection method to locate the critical point **C** : $\mathbf{u}_{cr}$, $t_{cr} = (u_M)_{cr}$. If it is a limit point, then go to step 5 . If it is a bifurcation point, then switch to the bifurcated equilibrium paths : choose $F_M = 0$ as in eqn (33) and solve the nonlinear equilibrium equations $\mathbf{F}(\mathbf{u}) = \mathbf{0}$ after the load step from time t_{cr} to time t by Broyden's method, and then go to step 5 .

5 . *Checking conditions for switching loading segments and for terminating tracing equilibrium paths.* (1) If $t < t_b$, where $t_b = 1.0$ for loading paths I, IV and for the second segments of loading paths II, III, V, VI, and $t_b = 0.5$ for the first segments of loading paths II, III, V, VI, then continue tracing equilibrium paths ; go to step 2 . (2) If $t > t_b$, then specify $t = t_s = t_b$, choose $F_M = 0$ as in eqn (34) and solve the nonlinear equilibrium equations $\mathbf{F}(\mathbf{u}) = \mathbf{0}$ within the load step from time $t - \Delta t$ to time t_b by Broyden's method. If $t_b = 0.5$, switch to the second segments of loading paths and continue tracing equilibrium paths : go to step 2 . If $t_b = 1.0$, terminate tracing equilibrium paths.

5. EXAMPLES

5.1. *Under different loading paths of* $\bar{p}_x$ and $\bar{p}_z$

The algorithm is applied in four representative examples of imperfect plates under three different loading paths of uniaxial compressive stress $\bar{p}_x$ and symmetric transverse load $\bar{p}_z$. In all these examples, $\gamma = 1.0$; $N = 4$; $(m_i, n_i) = (1, 1), (1, 3), (3, 1), (3, 3)$; $\bar{w}_{0i} = 0.2, 0.0, 0.0, 0.0$; $\bar{p}_x^* = 8.0$, $\bar{p}_y = 0$; and $\bar{q}_{ni} = 1, 1\ 3, 1\ 3, 1\ 9$ are selected, and only $\bar{p}_z^*$ is varied. The fundamental equilibrium paths $\bar{W}_1 - t$ under different loading paths of $\bar{p}_x$ and $\bar{p}_z$ are shown in Fig. 1(a), (b), (c), (d), respectively.

In Fig. 1(a), $\bar{p}_z^* = 1.20$; all loading paths I, II, III lead to final equilibrium state **A**: $\bar{W}_i^* = 1.9978, 0.0399, 0.0783, 0.0102$.

In Fig. 1(b), $\bar{p}_z^* = -0.80$; on the fundamental equilibrium path corresponding to loading path III, there is a bifurcation point **C**: $t_{cr} = 0.7500$, $\bar{p}_{xcr} = 3.9994$, $\bar{p}_{zcr} = -0.8000$, $\bar{W}_{icr} = 0.1950, -0.0028, -0.0042, -0.0003$; through the bifurcation point there are two stable bifurcated equilibrium paths which approach final equilibrium state **A**: $\bar{W}_i^* = 1.7746, 0.0255, 0.0538, 0.0051$ and state **B**: $\bar{W}_i^* = -1.7819, -0.0300, -0.0628, -0.0066$, respectively; loading paths I, II lead to final equilibrium state **A**.

In Fig. 1(c), $\bar{p}_z^* = -1.59$; on the fundamental equilibrium path corresponding to loading path I, there is a bifurcation point **C**: $t_{cr} = 0.5029$, $\bar{p}_{xcr} = 4.0230$, $\bar{p}_{zcr} = -0.7996$, $\bar{W}_{icr} = 0.2368, -0.0027, -0.0041, -0.0003$; through the bifurcation point there are

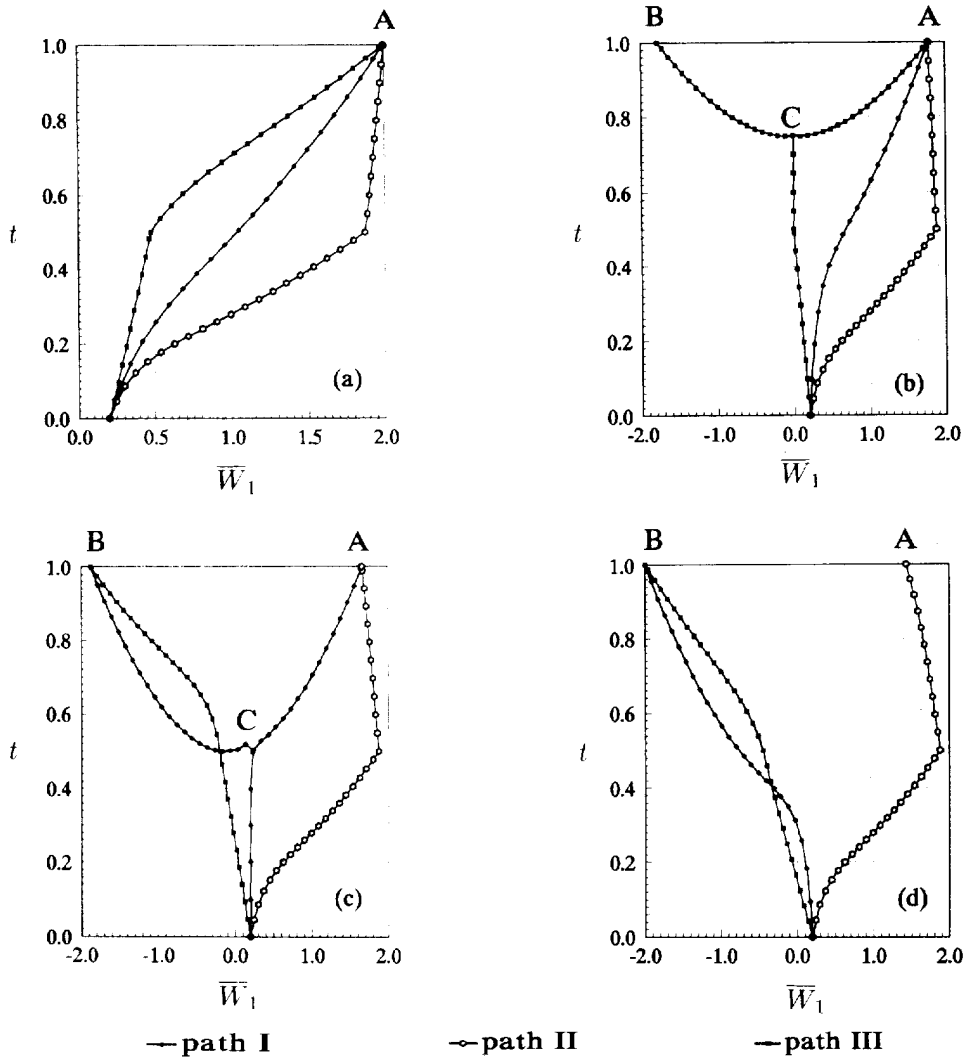

Fig. 1. Equilibrium paths under different loading paths of $\bar{p}_x$ and $\bar{p}_z$

two stable bifurcated equilibrium paths which approach final equilibrium state **A**: $\bar{W}_i^* = 1.6593,\ 0.0191,\ 0.0418,\ 0.0030$ and state **B**: $\bar{W}_i^* = -1.8780,\ -0.0358,\ -0.0728,\ -0.0086$, respectively; loading path II leads to final equilibrium state **A**; loading path III leads to final equilibrium state **B**.

In Fig. 1(d), $\bar{p}_2^* = -2.70$; loading path II leads to final equilibrium state **A**: $\bar{W}_i^* = 1.4339,\ 0.0085,\ 0.0201,\ 0.0002$; loading paths I, III lead to final equilibrium state **B**: $\bar{W}_i^* = -1.9937,\ -0.0434,\ -0.0852,\ -0.0115$.

Remark 3. Convergence tests have shown that taking $N = 4$ in these examples is accurate enough. For example, when taking $N = 9$; $(m_i, n_i) = (1, 1),\ (1, 3),\ (3, 1),\ (3, 3),\ (1, 5),\ (5, 1),\ (3, 5),\ (5, 3),\ (5, 5)$; $\bar{w}_{0i} = 0.2,\ 8{*}0.0$; $\bar{q}_{0i} = 1\ (m_i n_i)$, the final equilibrium states corresponding to Fig. 1(d) are

State **A**: $\bar{W}_i^* = 1.4338,\ 0.0085,\ 0.0200,\ 0.0002,\ -0.0007,\ -0.0009,\ -0.0002,\ -0.0002,\ -0.0001$;

State **B**: $\bar{W}_i^* = -1.9939,\ -0.0435,\ -0.0854,\ -0.0116,\ -0.0011,\ -0.0019,\ -0.0006,\ -0.0007,\ -0.0001$.

Remark 4. It is observed that under some loading paths with specially chosen final transverse loads, there exist bifurcation points on fundamental equilibrium paths even for imperfect plates, and through a bifurcation point there are two stable bifurcated equilibrium paths which approach different final equilibrium states. It is also observed that the final equilibrium states are to some extent sensitive to the final transverse loads. These phenomena may be explained generally by the multiplicity, sudden jumping and divergence features of a catastrophe, namely the double-cusp catastrophe [see, e.g., Thompson (1984) and Wicks (1988)]. These phenomena may also be enunciated specifically for these examples as follows. On the one hand, if the transverse load is applied in the same direction as the initial deflection, it is obvious that both the inplane compressive stress and the transverse load amplify the deflection, so different loading paths lead to the identical final equilibrium state [see Fig. 1(a)]. On the other hand, if the transverse load is applied in the opposite direction to the initial deflection, the inplane compressive stress amplifies the deflection, whereas the transverse load decreases the deflection, so it is possible that on a loading path either the compressive stress or the transverse load dominates the deflection (see Fig. 1(b), (c), (d)); it is also possible that on a loading path within some load range the compressive stress and the transverse load balance against each other, and at a critical load the balance breaks out (see equilibrium path III in Fig. 1(b) and equilibrium path I in Fig. 1(c)).

5.2. *Under different loading paths of* $\bar{p}_x$ and $\bar{p}_y$

The algorithm is also applied in eight examples of plates with different modes of initial deflection under three different loading paths of biaxial compressive stresses $\bar{p}_x$ and $\bar{p}_y$. In all these examples, $\gamma = 2.0$; $N = 9$; $(m_i, n_i) = (i, 1)$, $(i = 1, \ldots, N)$; $\bar{p}_x^* = 10.0, \bar{p}_y^* = 2.0$, $\bar{p}_z = 0.0$; $\bar{w}_{0i} = 0$, $(i = 4, \ldots, 9)$ are selected, and only $\bar{w}_{0i}$, $(i = 1, 2, 3)$ are varied permutedly.

The results are summarized in Table 1, where SO signifies initial states with $\bar{W}_i = \bar{w}_{0i}$; A4, A5, A6, B4, B5, B6 signify final equilibrium states with $\bar{W}_i = \bar{W}_i^*$; and C4, C5, C6 signify bifurcation points with $\bar{W}_i = \bar{W}_{icr}$ and t_{cr} being the corresponding bifurcation loading parameter (B.L.P.). An example of how the contents in the table may be interpreted is as follows: in example E100, loading paths IV, VI lead to final equilibrium state A6; on the fundamental equilibrium path corresponding to loading path V, there is a bifurcation point C5, through which there are two stable bifurcated equilibrium paths which approach different final equilibrium states A5 and B5, respectively.

Remark 5. Convergence tests have shown that taking $N = 9$ in these examples is accurate enough. For example, when taking $N = 7$ in example E110, the final equilibrium states are

State A5: $\bar{W}_i^* = 0.0723,\ 2.5158,\ -0.0509,\ 0.0013,\ 0.0198,\ 0.1310,\ -0.0042$;

State A6: $\bar{W}_i^* = 2.7698,\ 0.0175,\ 0.8551,\ -0.0049,\ 0.1544,\ 0.0016,\ 0.0270$;

Table 1. Final equilibrium states and critical states under different loading paths of $\bar{p}_1$ and $\bar{p}_3$

Example no.	Path no.	State no.	Deflection $\bar{W}_1$	$\bar{W}_2$	$\bar{W}_3$	$\bar{W}_4$	$\bar{W}_5$	$\bar{W}_6$	$\bar{W}_7$	$\bar{W}_8$	$\bar{W}_9$	B.L.P. t_{cr}
E000	IV	S0	0.000	0.000	0.000	0.000	0.000	0.000	0.000	0.000	0.000	
		C4	0.000	0.000	0.000	0.000	0.000	0.000	0.000	0.000	0.000	0.431123
		A4	0.000	0.000	1.835	0.000	0.000	0.000	0.000	0.000	0.000	
		B4	0.000	0.000	1.835	0.000	0.000	0.000	0.000	0.000	0.000	
	V	C5	0.000	0.000	0.000	0.000	0.000	0.000	0.000	0.000	0.000	0.200000
		A5	0.000	2.421	0.000	0.000	0.000	0.000	0.000	0.000	0.000	
		B5	0.000	2.421	0.000	0.000	0.000	0.000	0.000	0.000	0.000	
	VI	C6	0.000	0.000	0.000	0.000	0.000	0.000	0.000	0.000	0.000	0.390625
		A6	2.740	0.000	0.856	0.000	0.153	0.000	0.026	0.000	0.004	
		B6	2.740	0.000	−0.856	0.000	−0.153	0.000	−0.026	0.000	−0.004	
E100	IV,VI	S0	0.100	0.000	0.000	0.000	0.000	0.000	0.000	0.000	0.000	
		A6	2.770	0.000	0.854	0.000	0.156	0.000	0.026	0.000	0.004	
	V	C5	0.288	0.000	0.012	0.000	0.000	0.000	0.000	0.000	0.000	0.213547
		A5	0.069	2.489	−0.052	0.001	0.020	0.129	−0.004	0.000	0.001	
		B5	0.069	−2.489	−0.052	0.001	0.020	−0.129	−0.004	−0.000	0.001	
E010	IV,V	S0	0.000	0.100	0.000	0.000	0.000	0.000	0.000	0.000	0.000	
		A5	0.000	2.448	0.000	0.000	0.000	0.000	0.000	0.000	0.000	
	VI	C6	0.000	0.168	0.000	0.000	0.000	0.000	0.000	0.000	0.000	0.411958
		A6	2.741	0.014	0.857	0.004	0.153	0.001	0.026	−0.000	0.004	
		B6	−2.741	0.014	−0.857	−0.004	−0.153	0.001	0.026	−0.000	−0.004	

		S0	0.000	0.000	0.100	0.000	0.000	0.000	0.000	0.000	0.000	
	IV,V	A4	0.000	0.000	1.875	0.000	0.000	0.000	0.000	0.000	0.000	
E001		C6	0.000	0.000	0.118	0.000	0.000	0.000	0.000	0.000	0.000	0.401998
	VI	A6	2.728	0.000	0.903	0.000	0.142	0.000	0.029	0.000	0.004	
		B6	−2.746	0.000	−0.811	0.000	−0.163	0.000	−0.024	0.000	0.004	
		S0	0.100	0.100	0.000	0.000	0.000	0.000	0.000	0.000	0.000	
E110	IV,V	A5	0.073	2.516	-0.052	0.001	0.020	0.131	−0.004	0.000	0.001	
	VI	A6	2.770	0.018	0.855	−0.005	0.155	0.002	0.026	-0.000	0.004	
		S0	0.100	0.000	0.100	0.000	0.000	0.000	0.000	0.000	0.000	
E101	IV,VI	A6	2.757	0.000	0.904	0.000	0.145	0.000	0.029	0.000	0.004	
	V	A4	0.032	0.000	1.877	0.000	−0.007	0.000	0.002	0.000	0.012	
		S0	0.000	0.100	0.100	0.000	0.000	0.000	0.000	0.000	0.000	
E011	IV,V	A5	−0.293	2.481	0.264	0.034	−0.086	0.119	0.019	0.003	−0.003	
	VI	B6	−2.747	0.012	−0.813	−0.006	0.163	0.002	−0.024	−0.000	−0.004	
		S0	0.100	0.100	0.100	0.000	0.000	0.000	0.000	0.000	0.000	
E111	IV,V	A5	−0.225	2.496	0.218	0.022	−0.069	0.123	0.016	0.002	−0.002	
	VI	A6	2.757	0.020	0.905	−0.003	0.144	0.001	0.029	−0.000	0.004	

when taking $N = 9$, the final equilibrium states are

State A5: $\bar{W}_i^* = 0.0733,\ 2.5158,\ -0.0517,\ 0.0013,\ 0.0202,\ 0.1309,\ -0.0043,\ 0.0002,\ 0.0007$;

State A6: $\bar{W}_i^* = 2.7704,\ 0.0175,\ 0.8551,\ -0.0049,\ 0.1552,\ 0.0016,\ 0.0262,\ -0.0001,\ 0.0041$.

Remark 6. From the results, it is seen that there exist six different final equilibrium states with different dominant modes for the perfect plate, and there exist two or three different final equilibrium states close to the perfect states for the imperfect plates. Again, it is observed that under some loading paths with specially chosen initial deflections, there exist bifurcation points on fundamental equilibrium paths even for imperfect plates, and through a bifurcation point there are two stable bifurcated equilibrium paths which approach different final equilibrium states. This observation conforms to the results shown in Fig. 6 in Maaskant and Roorda (1992).

6. CONCLUDING REMARKS

For tracing equilibrium paths of simply supported rectangular thin plates in the nonlinear elastic range under different loading paths, a new algorithm is developed and applied in this paper. It is valid in all the following phases of tracing equilibrium paths: tracing primary equilibrium paths, locating critical (limit or bifurcation) points, switching from primary equilibrium paths to bifurcated equilibrium paths, tracing bifurcated equilibrium paths, and switching from one segment of loading paths to another. The algorithm is applied in some representative examples of imperfect plates under different loading paths.

Through these examples, the following phenomena are observed: (1) different loading paths of uniaxial compressive stress and transverse load or of biaxial compressive stresses sometimes lead to different final equilibrium states; (2) under some loading paths with special final loads, there exist bifurcation points on fundamental equilibrium paths even for imperfect plates, and through a bifurcation point there are two stable bifurcated equilibrium paths which approach different final equilibrium states; (3) the final equilibrium states are to some extent sensitive to the magnitudes of the transverse loads and to the modes of the initial deflection. These phenomena may be explained generally by the multiplicity, sudden jumping and divergence features of catastrophes.

For practical applications, the effects of influence parameters, such as aspect ratio, initial imperfections, inplane stresses and transverse load, should be studied systematically and the results should be discussed and summarized; however, these contents are not incorporated in this paper due to length limitations.

To complement, it is believed that the algorithm developed in this paper may be applied to other structures and members provided the nonlinear algebraic equilibrium equations are replaced accordingly. It is hoped that this study will contribute to an understanding of the phenomenon of multiple final equilibrium states and the phenomenon of mode jumping, and will guide nonlinear structural analysis.

Acknowledgements—This work is jointly supported by the National Natural Science Foundation and the Ministry of Construction of China which are gratefully acknowledged. Remarks were added in reply to the anonymous reviewers' comments which were helpful in revisions.

REFERENCES

Chia, C. Y. (1980). *Nonlinear Analysis of Plates*. McGraw-Hill, Inc., Scarborough, CA.

Dennis, J. E. Jr and Schnabel, R. B. (1983). *Numerical Methods for Unconstrained Optimization and Nonlinear Equations*. Prentice-Hall, New Jersey.

Maaskant, R. and Roorda, J. (1992). Mode jumping in biaxially compressed plates. *Int. J. Solids Struct.* **29**(10), 1209–1219.

Thompson, J. M. T. (1984). *Elastic Instability Phenomena*. Wiley, Chichester.

Wicks, P. J. (1988). A classification of behaviour in doubly-symmetric compound branching. *Int. J. Mech. Sci.* **30**(11), 821–833.